

# Anomalous penetration mechanisms of very intense laser pulses into overdense plasmas

Hitoshi Sakagami

*Computer Engineering, Himeji Institute of Technology, 2167 Shosha, Himeji, Hyogo 671-22, Japan*

Kunioki Mima

*Institute of Laser Engineering, Osaka University, 2-6 Yamada-oka, Suita, Osaka 565, Japan*

(Received 29 November 1995)

The interactions between very intense laser pulses and overdense plasmas are investigated with the use of a 1-1/2 dimensional electromagnetic, relativistic both for electron and ion, particle-in-cell code EMPAC. When the laser intensity increases, the laser front can penetrate into the plasma slab even if the plasma density is higher than the critical density. The propagation velocity of the laser front is compared with the analytical model and found to be significantly lower than the analytical result. The reason is attributed to the relaxation oscillation of electron density and recession velocity at the laser front. The intensity threshold for the penetration is found to depend on both plasma density and the electron-ion mass ratio. [S1063-651X(96)05308-1]

PACS number(s): 52.40.Nk, 52.35.Nx, 52.60.+h, 52.65.Cc

## I. INTRODUCTION

Recent developments of laser technology have made it possible to generate very intense subpicosecond pulses, and experiments are now being carried out to explore new regimes of relativistic laser-plasma interactions [1–3]. When the plasma is irradiated by such lasers with intensities up to  $I_L \lambda_L^2 \sim 10^{20}$  W  $\mu\text{m}^2/\text{cm}^2$ , electrons oscillating in the field of the laser wave are strongly relativistic. Here  $I_L$  is the laser intensity and  $\lambda_L$  is the wavelength in microns. The physics of interaction of such intense laser pulses with the plasmas substantially differs from that of the lower intensity cases. One of the most interesting applications envisaged for those laser systems is the fast ignitor [4]. The key concept of the fast ignitor is to heat the compressed hot core by suprathermal electrons and energetic ions generated by a very intense pulse, which is irradiated after a main laser pulse causes the implosion. In this scheme, the ignition laser must channel its way through a corona plasma and deposit its energy near the hot core for the efficient transport of suprathermal electrons and energetic ions to the fuel. To achieve this, one approach is to bore a hole through the corona plasma by a ponderomotive force associated with the drilling laser [5,6]. It was predicted that the intense laser pulse would be able to propagate into a sufficiently overdense plasma by the relativistic electron mass correction, which results in a decrease of the effective electron plasma frequency [7–9]. This anomalous penetration of the intense laser pulse through the corona plasma is another possibility to bring the ignition laser close to the compressed hot core. Recently, it was reported that an s-polarized wave interacting with a sharp-boundary plasma has excited an electromagnetic nonlinear pulse with relativistic amplitude propagating into the overdense plasma [10], and the transition between an opacity regime and a transparency regime for the propagation of the intense laser pulse into overdense plasmas has been discussed [11].

In this paper, we present the detailed mechanisms of the anomalous penetration of the intense laser pulse into an overdense plasma, up to twenty times a cutoff density. We simulated a linearly polarized electromagnetic wave irradiating a

homogeneous plasma at normal incidence, with the use of a 1-1/2 dimensional electromagnetic, relativistic both for electron and ion, particle-in-cell code EMPAC. The laser pulse is launched from the right boundary and ramped up to a given amplitude over a quarter of the laser period. The dense plasma slab, which is  $\sim 100\lambda_L$  long and thick enough not to become underdense by the expansion into vacuum during simulations, is introduced in the simulation system. The plasma consists of one species of singly ionized  $2 \times 10^5$  ions and  $2 \times 10^5$  electrons with initial temperatures  $T_e = 10$  keV and  $T_i = 10$  eV. Long ( $\sim 150\lambda_L$ ) vacuum regions are appended in both sides of the plasma slab. Therefore, no artificial boundary conditions, such as the reemission of escaping particles, are needed. In Sec. II, we investigate the relativistic electron dynamics with immobile ions. Though the threshold for the anomalous penetration and the recession velocity of the laser front have been discussed in Ref. [11], we investigate them with much larger ranges of the laser intensities and the plasma densities, and discuss the relaxation oscillation of the electron density coupling with the laser propagation in detail. A minute description about the dependence of the electron-ion mass ratio on the threshold laser intensity for the anomalous penetration is given in Sec. III. Section IV contains our summary.

## II. RELATIVISTIC ELECTRON DYNAMICS

When the effective electron plasma frequency is reduced below the laser frequency by increasing the inertial electron mass due to the relativistic effect, the laser pulse can penetrate into a classically overdense plasma [11]. The ion density and the laser field profiles obtained from a typical simulation result are shown in Fig. 1. The small density modulation in the region  $3000 < x/\lambda_{De} < 4200$  seems to be the thermal fluctuation for lack of particles per mesh, because the same noise levels are observed even if no laser is irradiated. Here  $\lambda_{De}$  denotes the electron Debye length. The laser front propagates deeply into the overdense plasma with a steady velocity, and that is called the “anomalous penetration.” We first perform our simulations with immobile ions

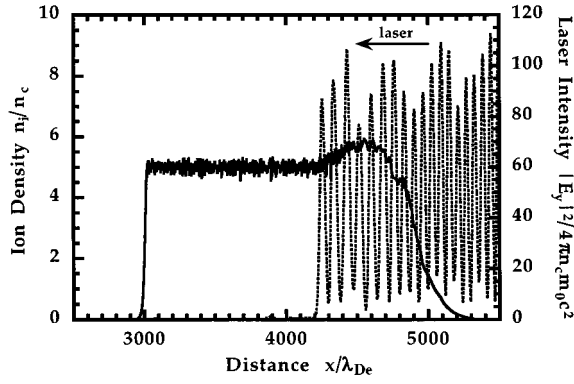


FIG. 1. The ion density (solid line) and the laser field profiles (dot line) obtained from a typical simulation result at  $\omega_{pe}t = 500$  for  $I_L \lambda_L^2 = 10^{20}$  W  $\mu\text{m}^2/\text{cm}^2$ ,  $m_i/m_e = 1836$ , and  $n_0/n_c = 5$ . The laser is launched from the right boundary.

to investigate a relativistic electron dynamics and characteristics of the anomalous penetration.

The analytic formula for a velocity of the laser front propagating into the plasma, which was simply derived as the group velocity of the relativistic intense laser pulse from the dispersion relation, can be given as follows:

$$\frac{v_{\text{prop}}}{c} = \left(1 - \frac{n_0}{n_c \gamma}\right)^{1/2}, \quad (1)$$

where  $v_{\text{prop}}$  is the propagation velocity,  $c$  is the light speed in vacuum,  $n_0$  is the plasma density,  $n_c$  is the critical density, and  $\gamma$  is the Lorentz factor. Ignoring the oscillation in the longitudinal field and considering only the quivering velocity in the transverse field, the simple estimation for  $\gamma$  is obtained as follows [5]:

$$\gamma = \left(1 + \frac{I_L \lambda_L^2}{1.37 \times 10^{18}}\right)^{1/2}. \quad (2)$$

Simulations with immobile ions, in which the ion inertia has no effect, are performed to estimate the threshold of the laser intensity for the anomalous penetration with different plasma densities. Figure 2 shows the transition between the anomalous penetration regime and the reflection regime depending on the plasma density as a function of the laser intensity. Those transitions were determined from the electron density and the laser field profiles at  $\omega_{pe}t = 200$  or  $\omega_L t = 89$  since the laser strikes the plasmas, where  $\omega_{pe}$  and  $\omega_L$  are the electron plasma frequency and the laser frequency, respectively. The laser was reflected at the plasma edge that was fixed due to immobile ions in case of the reflection, but the laser penetrated into the plasma and the electron density modulation was observed behind the laser front in the other case. The analytic formula is obtained from Eq. (1) with  $v_{\text{prop}} = 0$ , where the region below the analytic curve indicates the anomalous penetration regime. There is remarkable agreement between them. Thus we can conclude that the relativistic effect plays a dominant role in the mechanism of the anomalous penetration [11].

The propagation velocities can be measured from the trajectories of the laser front, and are shown in Fig. 3 for two different plasma densities as a function of the laser intensity.

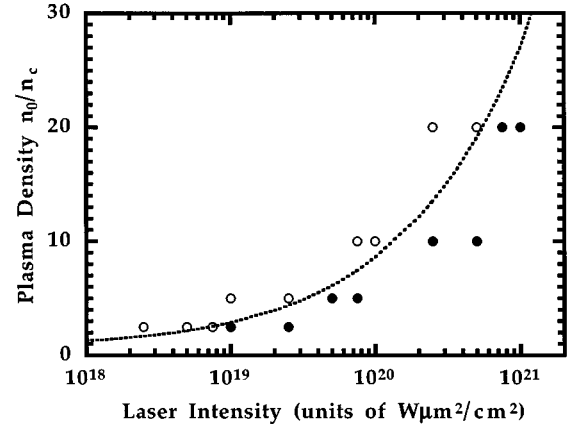


FIG. 2. The transition diagram between the anomalous penetration and the reflection for immobile ions depending on the plasma density as a function of the laser intensity. Solid, hollow circles, and dot line indicate the penetration, the reflection, and the analytic formula, respectively.

The propagation velocity increases with the laser intensity for a given plasma density, and decreases as the plasma density increases if the laser intensity is fixed. We found that there were large discrepancies between the simulation results and the analytic formula given in Eq. (1). Namely, the velocity obtained by simulations is significantly lower than the analytical prediction. It is noted that both the threshold intensity and the propagation velocity have a good agreement with the results in Ref. [11] in specific parameters.

As the laser pulse propagates through the plasma, electrons are pushed by the light pressure. This pressure is generated by the oscillating component of the ponderomotive force of frequency  $2\omega_L$  [12], and accumulates electrons at the propagating laser front. Accumulation of electrons leads to an increase in the electron density as long as the ponderomotive force exceeds the thermal pressure, hence to a decrease in the propagation velocity of the laser front. When the electron density overcomes the threshold density for the

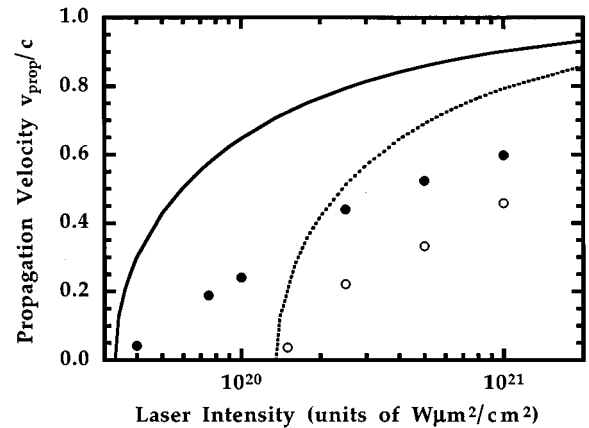


FIG. 3. The propagation velocity with immobile ions as a function of the laser intensity. Solid and hollow circles represent the simulation results for  $n_0/n_c = 5$  and  $n_0/n_c = 10$ , respectively, and solid and dot lines represent the analytic formula for  $n_0/n_c = 5$  and  $n_0/n_c = 10$ , respectively.

anomalous penetration, the laser pulse cannot even anomalously penetrate into the plasma and is finally reflected. The electron aggregation at the laser front also conducts to form a strong charge separation and to generate a large electrostatic field there. Since the ponderomotive force is oscillating, it becomes to be below the sum of the thermal pressure and the electrostatic force at a certain period. Then electrons run away from the laser front region, decreasing the electron density and the laser penetrates into the plasma again. Thus the electron density oscillates with the ponderomotive force and the same processes described above are repeated. They cause the relaxation oscillation of the propagation velocity that is coupled with the electron density oscillation. The  $x$ - $t$  diagrams of the electron density, the electromagnetic field intensity, and the electrostatic field intensity for  $I_L \lambda_L^2 = 2.5 \times 10^{20} \text{ W } \mu\text{m}^2/\text{cm}^2$  are shown in Figs. 4(a), 4(b), and 4(c), respectively. The threshold density of that laser intensity is  $n_0/n_c = 13.5$  and the regions in which the electron density is more than that value are displayed as black in Fig. 4(a). The electron accumulation and runaway at the laser front are shown, and the wagging narrow overcritical peaks also appear in the underdense region behind the laser front [13]. It is clearly seen that the laser is reflected at  $n_0/n_c > 13.5$  regions, and the incident and reflected laser cancel out each other at the high density point, forming an interference pattern in the rest area in Fig. 4(b). The electron density obviously shows the relaxation oscillation coupling with the laser that repeats the anomalous penetration and the reflection by turns. The electrostatic field is also found to be strong at that point due to the charge separation and to vibrate with the electron density oscillation from Fig. 4(c). The electron density modulations also exist in the underdense region behind the laser front, where the laser light is reflected through the ‘‘coherent scattering.’’

The trajectory of the laser front and the electron density at the laser front are shown in Fig. 5, clearly representing the relaxation oscillation. The laser can travel into the plasma with the velocity predicted by Eq. (1) only in a moment, but the velocity is quickly reduced. The propagation velocities obtained in Fig. 3 are evaluated by a time average of the oscillating trajectory of the laser front, so they are reasonably calculated to be below the analytical predictions. It is noted that the oscillation frequency is shifted to the red due to the propagation of the laser front and can be calculated with the usual Doppler formula as  $\omega = 2\omega_L (1 - v_{\text{prop}}/c) = 1.2\omega_L$ . This frequency agrees well with the oscillation period in Fig. 5.

### III. ION DYNAMICS

We have also performed the simulations with different electron-ion mass ratios to investigate the effect of the ion inertia to the anomalous penetration. The transitions between the anomalous penetration regime and the reflection regime depending on the electron-ion mass ratio as a function of the laser intensity are also shown in Fig. 6(a) for  $n_0/n_c = 5$  and in Fig. 6(b) for  $n_0/n_c = 10$ . In those cases, the transitions were also determined by the same criteria used for Fig. 2. A vertical dash line indicates the analytic threshold for corresponding parameters obtained from Fig. 2, where the right part of the line is the anomalous penetration regime. It is

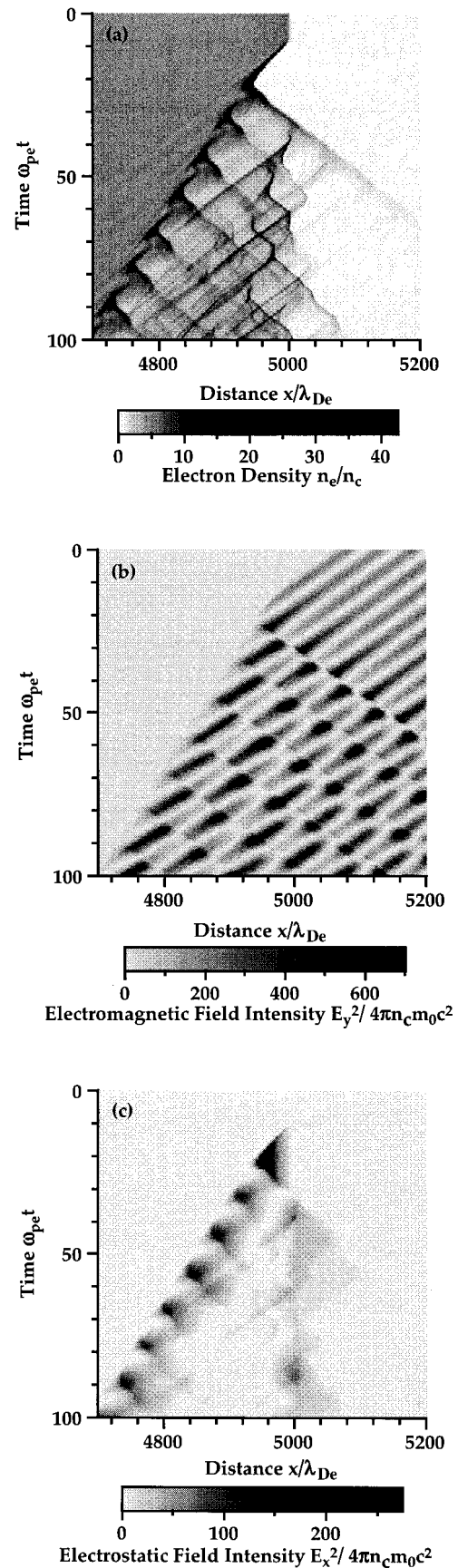


FIG. 4. The  $x$ - $t$  diagrams of (a) the electron density, (b) the electromagnetic field intensity, and (c) the electrostatic field intensity for  $I_L \lambda_L^2 = 2.5 \times 10^{20} \text{ W } \mu\text{m}^2/\text{cm}^2$  and  $n_0/n_c = 5$  with immobile ions.

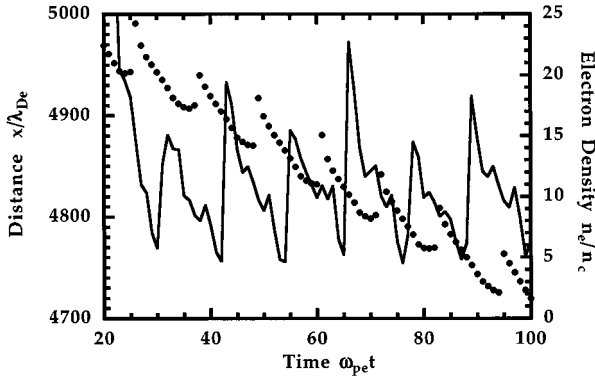


FIG. 5. The trajectory of the laser front (solid circle) and the time evolution of the electron density at the laser front (solid line) for  $I_L \lambda_L^2 = 2.5 \times 10^{20} \text{ W } \mu\text{m}^2/\text{cm}^2$  and  $n_0/n_c = 5$  with immobile ions.

clearly seen that light ions prevent the laser from invading into the overdense plasma even though its intensity is greater than the threshold intensity, and the higher the laser intensity is, the lighter ion is needed for the infiltration [11].

When the laser intensity is greater than the threshold that

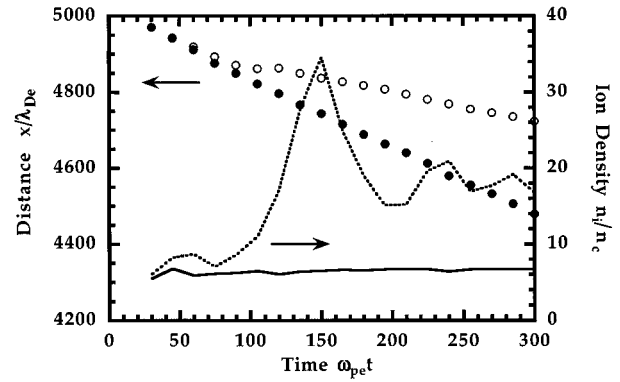


FIG. 7. The trajectory of the laser front (circles) and the time evolution of the ion density at the laser front (lines) for  $I_L \lambda_L^2 = 10^{20} \text{ W } \mu\text{m}^2/\text{cm}^2$  and  $n_0/n_c = 5$ . Solid circles and solid line represent the simulation results as a case of the anomalous penetration with  $m_i/m_e = 1000$ , hollow circles and dot line as a case of the reflection with  $m_i/m_e = 500$ .

is predicted by Eq. (1) for the initial plasma density, quivering electrons increase their inertial mass and hence decrease the effective electron plasma frequency below the laser frequency. Thus the laser pulse does not reflect at the plasma edge and can penetrate into the plasma regardless of the electron-ion mass ratio. Electrons are accumulated by the ponderomotive force that is generated by the penetrating laser and the electron density increases at the laser front, but the ion density endures its initial value. A large electrostatic field is generated by the strong charge separation and propagates together with the laser front. When the ion is too heavy to catch up with the propagating electrostatic field, the laser pulse continues to penetrate into the plasma. But if the ion is light enough to react with the electrostatic field, ions are also accumulated at the laser front and the ion density increases there. Thus the laser pulse is reflected by the narrow overcritical plasma peak after the ion density overcomes the threshold density that is obtained by Eq. (1) for the irradiated laser intensity [13]. Once ions are assembled, the overcritical plasma peak does not fade away and the laser pulse is continuously reflected. The trajectory of the laser front and the time evolution of the ion density at the laser front are shown in Fig. 7 for both the anomalous penetration and the reflection cases, with the incident laser intensity  $I_L \lambda_L^2 = 10^{20} \text{ W } \mu\text{m}^2/\text{cm}^2$ . In the anomalous penetration case, the ion density is always below the threshold density ( $n_0/n_c = 8.6$ ) and the laser front propagates into the plasma at a steady speed. As for the reflection case, the ion density increases and overcomes the threshold density around  $\omega_{pe}t = 100$ , and then the laser pulse is reflected by the plasma peak and its front propagates with a different velocity, which can be estimated by balancing the momentum flux of the mass flow with the laser pressure. Once the laser pulse is reflected, the collisionless shock is launched by the extremely high pressure of the reflected laser pulse, compressing the plasma, and the ion density quickly increases much more than the threshold density. It is noted that the positions of the laser front in Fig. 7 are obtained by the time average over the laser period and thus no oscillation can be found, unlike in Fig. 5.

An ion acoustic speed is determined by an electron temperature and an ion mass. In our cases of the laser intensity

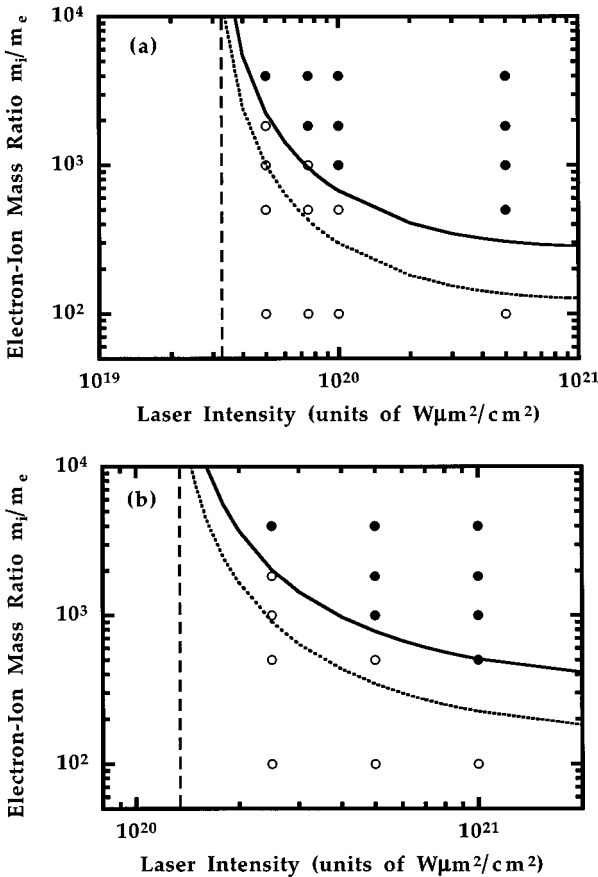


FIG. 6. The transition diagram between the anomalous penetration and the reflection depending on the electron-ion mass ratio as a function of the laser intensity for (a)  $n_0/n_c = 5$  and (b)  $n_0/n_c = 10$ . Solid and hollow circles represent the penetration and the reflection, respectively, dot and solid lines represent factor  $f = 1.0$  and  $1.5$ , respectively, and vertical dash lines indicate the threshold laser intensities for given plasma densities.

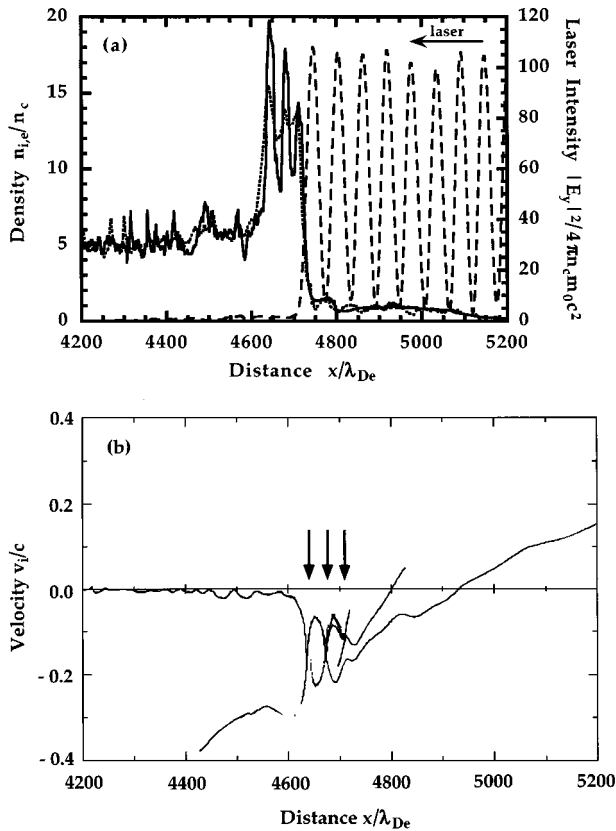


FIG. 8. The plasma structures of the reflection case with  $m_i/m_e=500$  at  $\omega_{pe}t=300$  for  $I_L\lambda_L^2=10^{20}$  W  $\mu\text{m}^2/\text{cm}^2$  and  $n_0/n_c=5$ . (a) The ion density (solid line), the electron density (dot line), and the laser field profiles (dash line), and (b) the ion phase space. Arrows indicate the position of the peaks in the ion density profile.

( $I_L\lambda_L^2 > 10^{19}$  W  $\mu\text{m}^2/\text{cm}^2$ ), a significant fraction of the light energy is absorbed into suprathermal electrons with an effective temperature of more than  $\sim 1$  MeV, which is much higher than the background electron temperature of 10 keV [5,14]. Thus the suprathermal electron temperature can mainly determine the ion acoustic speed. A precise treatment for the suprathermal electron temperature greatly complicates the estimation, but the suprathermal electron temperature can be approximately estimated from the quivering velocity in the laser field with a simple formula [5]. Though this leads to underestimation because it does not include the energy of oscillation in the longitudinal field, it provides a reasonable characteristic temperature for the suprathermal electrons. To avoid the complexity, we use this simple equation to obtain the suprathermal electron temperature as a function of the laser intensity and introduce a calculation factor with a value of greater than unity, which compensates the crude estimation.

As the ion motion can be scaled by the ion acoustic speed, we can estimate the transitional condition between the anomalous penetration and the reflection as follows:

$$v_{\text{prop}} = f c_{\text{sh}}, \quad (3)$$

where  $v_{\text{prop}}$  is the propagation velocity of the laser front that is evaluated by the interpolation with the simulation results,

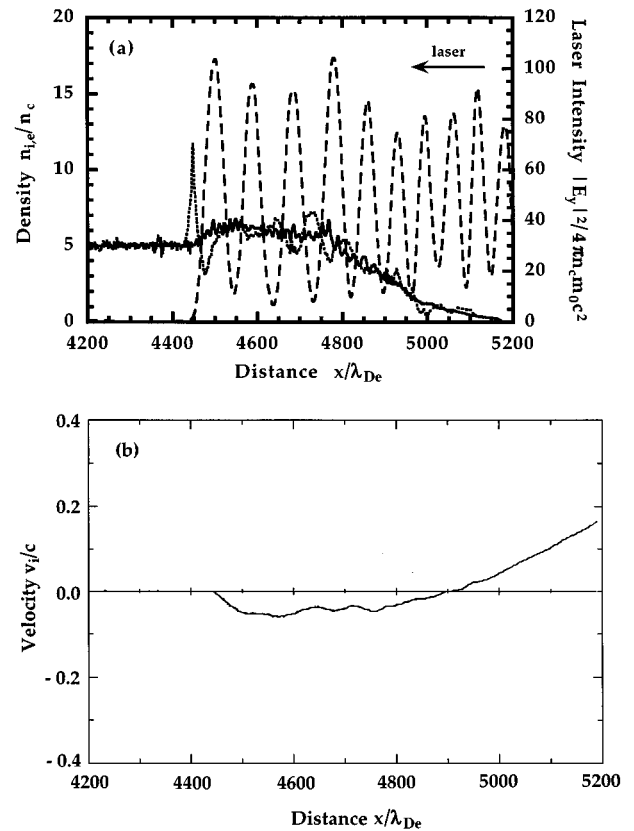


FIG. 9. The plasma structures of the anomalous penetration case with  $m_i/m_e=1000$  at  $\omega_{pe}t=300$  for  $I_L\lambda_L^2=10^{20}$  W  $\mu\text{m}^2/\text{cm}^2$  and  $n_0/n_c=5$ . (a) The ion density (solid line), the electron density (dot line), and the laser field profiles (dash line), and (b) the ion phase space.

$c_{\text{sh}}=(T_{\text{he}}/m_i)^{1/2}$  is the ion acoustic speed,  $T_{\text{he}}=(\gamma-1)m_e c^2$  is the suprathermal electron temperature,  $m_i$  ( $m_e$ ) is the ion (electron) mass, and  $f$  is a calculation factor due to the crude estimation for  $T_{\text{he}}$ . The transitional curves are shown in Figs. 6 for  $f=1.0$  (dot line) and 1.5 (solid line). For both  $n_0/n_c=5$  and  $n_0/n_c=10$  cases, the curves for  $f=1.5$  agree quite well with the simulation results, better than those for  $f=1.0$ . We cannot discuss an absolute value of  $f$  here, but we can conclude that the effect of the ion inertia to the anomalous penetration is characterized by the ion acoustic speed with the suprathermal electron temperature.

In the reflection regime, the very intense laser pulse strikes the plasma slab and electrons are pushed by the extremely high pressure of the laser. Then the collisionless shock is launched and propagates into the plasma. The large electrostatic field is generated at the reflection front by the strong charge separation and produces a very energetic ion beam inward [5,15]. The ion density, the electron density, and the laser field profiles are shown in Fig. 8(a), and the ion phase space in Fig. 8(b) for the reflection case with the same simulation parameters as in Fig. 7. It is clearly seen that the ion beam is generated and propagates into the plasma ahead of the shock. At this time, the incident laser is reflected by the plasma edge around  $x/\lambda_{De} \sim 4720$  and the collisionless shock front is found around  $x/\lambda_{De} \sim 4630$ , where the ion beam is launched. The velocity of the plasma edge ( $u_e$ ) can be estimated as  $u_e/c \sim 0.12$  by balancing the momentum flux

of the mass flow with the laser pressure [5,15], and agrees with the simulation result of  $u_e/c \sim 0.13$  and a red shifting in frequency of the reflected light. The shock propagates with the constant velocity of  $u_s/c \sim 0.17$ , and compress the plasma more than twice the initial density. Three peaks of the ion density are found in the compressed plasma, corresponding to bounds of a hole in the ion phase space, and the number of the holes, which is two in this case, coincides with the period of the ion plasma oscillation; i.e.,  $t = 300/\omega_{pe} = 13.4/\omega_{pi} \sim 2(2\pi/\omega_{pi})$ , where  $\omega_{pi}$  is the ion plasma frequency. Momentum conservation requires the velocity of the ion beam ( $u_b$ ) to be twice the plasma edge velocity; i.e.,  $u_b/c \sim 0.26$ , but Fig. 8(b) shows that ions are much more accelerated than that value due to the presence of the collisionless shock.

On the other hand, no energetic ion beam is generated for the case of anomalous penetration. The ion density, the electron density, and the laser field profiles are also shown in Fig. 9(a), and the ion phase space in Fig. 9(b) for the anomalous penetration case with the same simulation parameters as in Fig. 7. The laser front, which is propagating into the plasma with  $v_{prop}/c \sim 0.25$ , is found around  $x/\lambda_{De} \sim 4460$ . Electrons are accumulated ahead of the laser front, but the region just behind the laser front has a lack of electrons. This arrangement generates the electrostatic field, which accelerates ions up to  $v_i/c \sim 0.05$ . The inward ion velocity is much slower than the propagation velocity of the laser front, thus unperturbed ions are successively accelerated at the laser front, forming a beamlike distribution in phase space. It is

noted that ions are pulled by blown off electrons and are expanding into the vacuum toward the incoming laser in both cases.

#### IV. SUMMARY

We have investigated, through a series of simulations with the 1-1/2 dimensional electromagnetic, relativistic particle-in-cell code EMPAC, the anomalous penetration, namely, the laser pulse could propagate into a classically opaque overdense plasma by increasing the inertial electron mass and hence decreasing the effective electron plasma frequency. If ions have infinite mass and the ion inertia has no effect, we have found that the analytical thresholds of the anomalous penetration were in good agreement with simulation results. It was also found that the recession velocity was significantly reduced due to the relaxation oscillation of the penetration that is coupled with the electron density oscillation at the laser front.

As a finite ion mass, light ions were found to raise the threshold intensity of the anomalous penetration for a fixed plasma density, and this mechanism could be explained by the ion dynamics that was characterized by the ion acoustic speed.

#### ACKNOWLEDGMENT

We would like to thank Professor K. Nishihara, Dr. S. Kato, and S. Miyamoto for fruitful discussions.

- 
- [1] P. Main and G. Mourou, *Opt. Lett.* **13**, 467 (1988).
  - [2] M. D. Perry, F. G. Patterson, and J. Weston, *Opt. Lett.* **15**, 381 (1990).
  - [3] F. G. Patterson, R. Gonzales, and M. D. Perry, *Opt. Lett.* **16**, 1107 (1991).
  - [4] M. Tabak, J. Hammer, M. E. Glinsky, W. L. Kruer, S. C. Wilks, J. Woodworth, E. M. Campbell, and M. D. Perry, *Phys. Plasma* **1**, 1626 (1994).
  - [5] S. C. Wilks, W. L. Kruer, M. Tabak, and A. B. Langdon, *Phys. Rev. Lett.* **69**, 1383 (1992).
  - [6] S. C. Wilks, *Phys. Fluids B* **5**, 2603 (1993).
  - [7] A. I. Akhiezer and P. V. Polovin, *Sov. Phys. JETP* **3**, 696 (1956).
  - [8] P. Kaw and J. Dawson, *Phys. Fluids* **13**, 472 (1970).
  - [9] A. D. Steiger and C. H. Woods, *Phys. Rev. A* **5**, 1467 (1972).
  - [10] S. V. Bulanov, N. M. Naumova, and F. Pegoraro, *Phys. Plasmas* **1**, 745 (1994).
  - [11] E. Lefebvre and G. Bonnaud, *Phys. Rev. Lett.* **74**, 2002 (1995).
  - [12] P. Sprangle, E. Esary, and A. Ting, *Phys. Rev. Lett.* **64**, 2011 (1990).
  - [13] M. P. Kalashnikov, P. V. Nickles, Th. Schlegel, M. Schnuerer, F. Billhardt, I. Will, and W. Sandner, *Phys. Rev. Lett.* **73**, 260 (1994).
  - [14] P. Gibbon, *Phys. Rev. Lett.* **73**, 664 (1994).
  - [15] J. Denavit, *Phys. Rev. Lett.* **69**, 3052 (1992).